

# Investigation of Quark–Antiquark Interaction Properties using Leading Particle Measurements in $e^+e^-$ Annihilation

Martin Erdmann

Institut für Experimentelle Kernphysik, Universität Karlsruhe,  
Wolfgang-Gaede-Str. 1, D-76131 Karlsruhe  
Martin.Erdmann@cern.ch

## Abstract

Measurements of heavy quark production in electron–positron collisions are used to analyse the strong interactions between quarks and anti-quarks. A scaling behaviour is observed in distributions of the rapidity change of  $D^*$ ,  $B^*$ , and B mesons. From these distributions information is obtained on the hadron formation time, effective quark masses, and the potential between quark–antiquark pairs. Predictions for fragmentation functions are presented.

*Phys. Lett. B 510 (2001) 29*

PACS: 13.65.+i

Key words:

*fragmentation, formation time, quark masses, strong interaction potential*

# 1 Motivation

Measurements of fragmentation processes imply that quarks are subjected to large energy losses from strong interactions before they form hadrons. The production of heavy quark–antiquark pairs at electron–positron colliders provides a suitable environment in which to analyse these strong interactions, namely, the initial state is colour neutral, and the initial kinematics is known from the beam energy. The final state momenta of the quarks are carried away by the measured D and B mesons, except for corrections due to the second quark which is required for hadron formation and higher meson resonances.

The perspective followed in this analysis is that the primary quark loses energy during the time it remains in the strong field originating from the primary quark and anti-quark travelling away from each other. The questions addressed are: how long did the quark remain in the field ? are there variations in the field strength ? what is the influence of the quark mass ? The answers will be used to predict fragmentation functions for particles which contain the primary quark and which have not decayed.

## 2 Rapidity Change

Instead of the fractional energy  $x = E_{hadron}/E_{beam}$ , commonly used in the studies of fragmentation data, the rapidity change  $\Delta y = y_i - y_f$  in the direction of motion is used in this analysis. We take advantage of the fact that  $\Delta y$  is the same in the laboratory and in the rest frame of the quark. The initial rapidity  $y_i$  of the quark with mass  $m$  is given by the  $e^+e^-$  center of mass energy  $\sqrt{s}$  via  $y_i = \ln(\sqrt{s}/m)$ . The quark final state rapidity is  $y_f$  and corresponds to that of the primary hadron. Throughout this analysis

$$\Delta y = -\ln x \quad (1)$$

will be used where  $\Delta y$  is, for the data considered in this analysis, a good approximation to the quark rapidity change as defined above.

In Fig. 1a, the shapes of distributions of the rapidity change  $\Delta y$  are shown for D\* meson production in non-resonant  $e^+e^-$  annihilation at  $\sqrt{s} = 10.6$  GeV [1, 2], and D\* production from  $c\bar{c}$  decays of the Z boson [3]. Also shown is B [4] and B\* [5] meson production from Z decays to  $b\bar{b}$ . All data exhibit a maximum at small rapidity losses  $\Delta y_m$ . Above the maximum, the measurements can be described by exponentially falling dependences. In the case of the B meson measurement (full circles), two exponential components are visible in the data of which the first is likely to reflect primary B mesons, since the B\* meson data (star symbols) show a similar dependence. The measurements with the smaller slope at large  $\Delta y$  are presumably due predominantly to B mesons from resonance decays and are not further considered in this analysis.

The curves show fits to the data of the form

$$\left[ \frac{1}{N_{norm}} \frac{dN}{d\Delta y} \right]_i = A_i \exp \left( -\frac{\Delta y}{\Delta y_o} \right). \quad (2)$$

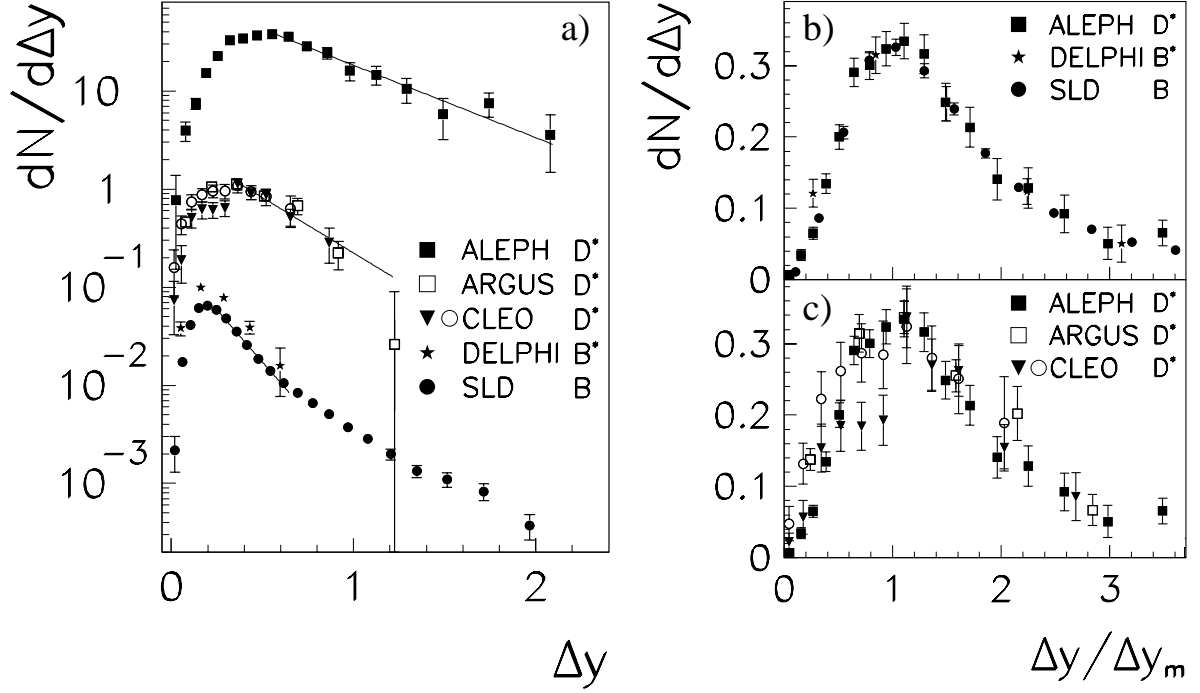


Figure 1: a) Shapes of distributions of the rapidity change  $\Delta y$  are shown for  $D^*$ ,  $B^*$ , and  $B$  mesons. The curves represent exponential fits. b,c) The same spectra of the rapidity change are shown, normalized to the rapidity change  $\Delta y_m$  where the distributions are maximal.

Experiment	Energy [GeV]	Meson	$1/\Delta y_o$	$1/\Delta y_m$	$N_{q,o}/N_{norm}$	$C$
ARGUS	10.6	$D^*$	$2.6 \pm 0.5$	$3.1 \pm 0.3$	$1.7 \pm 0.2$	$0.30 \pm 0.13$
CLEO					$81 \pm 10$	$0.50 \pm 0.13$
					$71 \pm 10$	$0.32 \pm 0.10$
ALEPH	$M_Z$	$D^*$	$1.7 \pm 0.2$	$2.0 \pm 0.1$	$[2.28 \pm 0.12] 10^{-3}$	$0.43 \pm 0.07$
SLD	$M_Z$	$B$	$4.9 \pm 0.2$	$5.2 \pm 0.1$	$0.935 \pm 0.012$	$0.49 \pm 0.05$

Table 1: Fit results of the exponential slope  $\Delta y_o$ , the rapidity change  $\Delta y_m$  at the maximum of the spectrum, the normalization  $N_{q,o}/N_{norm}$ , and the correction  $C$  for the start of the region where the strong force is constant.

A common exponential slope  $\Delta y_o$  was determined for each quark flavour and  $\sqrt{s}$  (Table 1). The normalizations  $A_i$  of each data set  $i$  were left free in these fits.

The values of the rapidity change  $\Delta y_m$ , at which the spectra are maximal, were also determined using a suitable fit (Table 1). Both characteristics of the spectra,  $\Delta y_m$  and  $\Delta y_o$ , give similar values which motivates tests of the similarity of the full spectra. In Fig. 1b,c all data are shown by multiplying the rapidity change with  $1/\Delta y_m$ . The measurements at the Z resonance are then found to follow a universal shape, independent of the quark flavour (Fig. 1b). At fixed quark flavour (Fig. 1c), the comparison of the measurements at different beam energies also

indicate similar shapes, except for the region of smallest  $\Delta y$  values. Although the errors of the data at the lower beam energy are large, they have the tendency to be above the measurements at the Z resonance.

The observation of a scaling behaviour in the spectra of the rapidity change is of interest and is suggestive of a common hadronization mechanism.

### 3 Proper Time

The distribution of the proper time  $\tau$ , measured in the rest frame of the quark, is related to the rapidity distribution by

$$\frac{dN}{d\tau} = \frac{dN}{d\Delta y} \frac{d\Delta y}{d\tau}. \quad (3)$$

The differential  $d\Delta y/d\tau$  is related to the acceleration of the quark. In the case of constant acceleration, the rapidity distribution gives a direct measure of the proper time distribution.

The region of large  $\Delta y$  in Fig. 1 corresponds to measurements at large distances between the quark–antiquark pair where the quark has remained in the field for a relatively long time interval. This long distance component of the strong interaction has been described by a constant force of strength  $\kappa \sim 1$  GeV/fm, e.g. [6], implying constant acceleration,

$$\frac{d\Delta y}{d\tau} \sim \frac{\kappa}{m} = \text{const.} \quad (4)$$

The  $\tau$ -distribution, corresponding to (2), is then exponentially distributed,

$$N_q = N_{q,o} \exp\left(-\frac{\tau}{\tau_o}\right). \quad (5)$$

Therefore, if the data at sufficiently large  $\Delta y$  reflect the rapidity losses due to a constant force, the proper time  $\tau$  is here exponentially distributed. This then implies that the probability for the appropriately coloured and flavoured light anti-quark appearing and joining with the heavy quark to form the hadron is constant with respect to the clock of the travelling heavy quark. A similar interpretation of  $\Delta y$  spectra has been suggested for  $pp \rightarrow pX$  [7] and  $\mu N \rightarrow J/\Psi X$  [8] data.

In what follows, we take the view that the mechanism behind fragmentation is probabilistic in nature and can be described by (5) with a universal formation time  $\tau_o$  which is independent of the strength of the force and the quark flavour.

### 4 Effective Quark Masses

One implication of a probabilistic fragmentation mechanism with a universal formation time  $\tau_o$  is the direct relation of the rapidity change spectra to the masses which are accelerated. From integration of (4) it follows that

$$m \sim \frac{\kappa\tau}{\Delta y} \sim \frac{\kappa\tau_o}{\Delta y_o}. \quad (6)$$

The different exponential slopes  $\Delta y_0$ , determined from the fits shown in Fig. 1, are then related to the different effective masses accelerated in the field. The energy scale is given by  $\kappa\tau_0$  which is expected to be of the order of 1 GeV.

In Fig. 2, the open symbols show results on the  $c$ - and  $b$ -quark masses at the corresponding energy  $\mu$ . The open square (circle) symbol gives the value of the  $c$  ( $b$ ) mass of reference [9]. The other open symbols result from 3-jet rate measurements in  $b\bar{b}$  events produced at the Z resonance ( [10] diamond symbol, [11] star symbol, [12] triangle symbol).

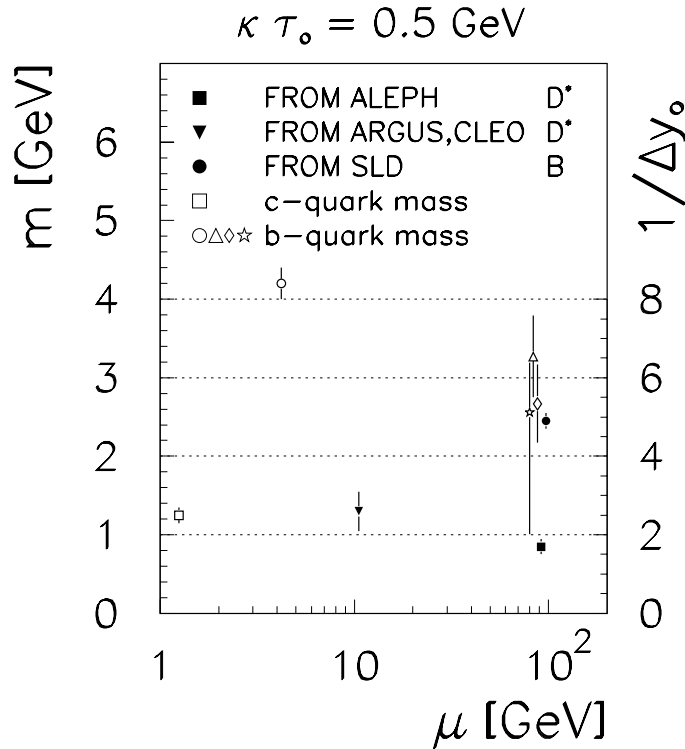


Figure 2: The inverse of the exponential slope  $\Delta y_0$  (right axis) is shown as a function of the beam energy  $\mu$  by the full symbols. The left axis gives the corresponding masses  $m$  using the energy scale  $\kappa\tau_0 = 0.5 \text{ GeV}$ . For comparison, determinations of the  $c$ - and  $b$ -quark masses are shown by the open symbols (see text).

The values of  $1/\Delta y_0$  are shown by the full symbols in the same diagram. The energy scale  $\kappa\tau_0 = 0.5 \text{ GeV}$  has been chosen, adjusting  $1/\Delta y_0$  of the  $D^*$  and  $B$  data to the  $c$ - and  $b$ -quark mass determinations respectively. The effective mass values of the  $D^*$  data are found to be consistently below the  $B$  data and indicate a dependence of the charm mass on the beam energy scale.

In this way, the observed scaling in the spectra of the rapidity change (Fig. 1) can naturally be explained by different quark masses being decelerated in the strong field.

## 5 Quark–Antiquark Interactions

A second implication of a probabilistic fragmentation mechanism with a universal formation time  $\tau_0$  is that variations in the strength of the force acting on the quarks can be determined as a function of the proper time. Taking the factor  $dN/d\tau$  in equation (3) from equation (5), integration of the measured rapidity spectra gives a relation between the rapidity change  $\Delta y$  and the proper time  $\tau$ ,

$$\tau(\Delta y) = -\tau_0 \ln \left( 1 - \frac{N_{norm}}{N_{q,\circ}} \int_0^{\Delta y} \left[ \frac{1}{N_{norm}} \frac{dN}{d\Delta y} \right] d\Delta y \right). \quad (7)$$

Since the experiments chose different procedures to normalize their data, the ratio  $N_{norm}/N_{q,\circ}$  is determined from the data at sufficiently large  $\Delta y$ , where (6) implies a linear relation between  $\Delta y$  and  $\tau$ ,

$$\frac{\tau}{\tau_0} = \frac{\Delta y}{\Delta y_0} - C. \quad (8)$$

Here  $C$  accounts for the start of the region where the force is constant. Replacing  $\tau/\tau_0$  in (7) by (8) allows  $N_{norm}/N_{q,\circ}$  and  $C$  to be determined (Table 1):

$$\int_0^{\Delta y} \left[ \frac{1}{N_{norm}} \frac{dN}{d\Delta y} \right] d\Delta y = \frac{N_{q,\circ}}{N_{norm}} \left( 1 - \exp \left( -\frac{\Delta y}{\Delta y_0} + C \right) \right). \quad (9)$$

In Fig. 3, the horizontal axis shows the proper time  $\tau$  in units of  $\tau_0$  from solving (7). The vertical axis gives the rapidity change  $\Delta y$ . It is multiplied by  $1/\Delta y_0$  to account for the observed scaling of the rapidity change spectra reported in section 2. The values of  $C$  are similar in the different data sets (Table 1). In Fig. 3a the long distance part is emphasized. It shows the linear relation between  $\Delta y$  and  $\tau$  which confirms the method of determining  $N_{norm}/N_{q,\circ}$ . At small distances, the rapidity loss is much larger per unit time.

Owing to the integration procedure, the points within a single experiment are correlated. Two errors are shown. The terminated errors give the range allowed by the uncertainty in  $N_{norm}/N_{q,\circ}$  and the other errors result from the errors of the original measurements. A simulation of the procedure showed that the simulated points reproduce the generated  $\Delta y(\tau)$  distribution except for a small overall shift in  $C$  from the integration using finite bin widths, and for the first point of the integration. This lowest point was omitted from the figure if the simulated displacement in  $\tau/\tau_0$  exceeded 100%.

Figure 3b shows the rapidity change as a function of the proper time on a logarithmic scale. The dashed curve indicates a linear rapidity loss. In the short distance region, the D\* and B measurements at the Z resonance are consistent with a dependence of  $\Delta y$  on the logarithm of  $\tau$ . The full curve attempts a parameterization as

$$\frac{\Delta y}{\Delta y_0} - C = a \ln \left( \frac{\tau}{\tau_0} \right) + b \left( \frac{\tau}{\tau_0} \right) + c \quad (10)$$

with  $a = 0.08$ ,  $b = 0.9$ , and  $c = 0.1$ . The D\* measurements at the smaller beam energy  $\sqrt{s} = 10.6$  GeV are also consistent with a logarithmic dependence, albeit with a tendency

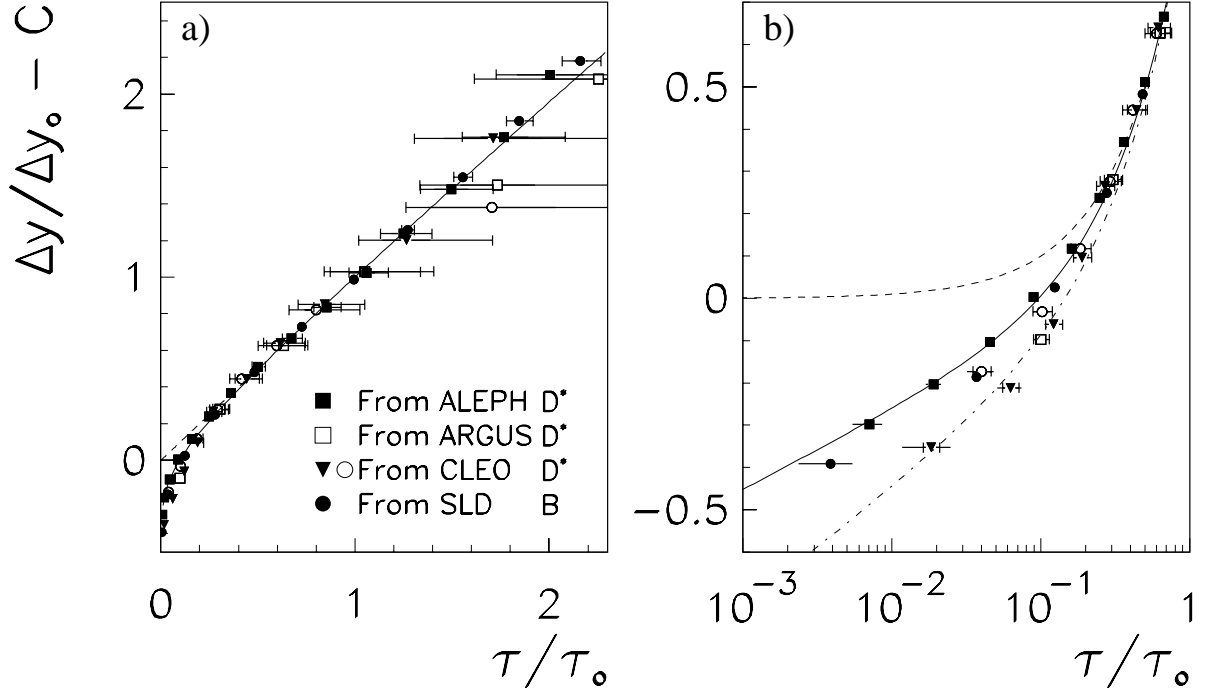


Figure 3: The rapidity change  $\Delta y$  of charm and bottom quarks, measured by  $D^*$  and B mesons from  $e^+e^-$  collisions, is shown as a function of the quark proper time  $\tau$ . The dashed curve denotes a linear dependence of  $\Delta y$  on  $\tau$  as expected for a constant force. The full curve represents a logarithmic dependence of  $\Delta y$  on  $\tau$  for the short distance part, and a linear dependence for the long distance part. The dash-dotted curve shows an increased strength of the logarithmic term.

towards a larger value of  $a$  shown by the dash-dotted curve with  $a = 0.12$ . In principle, a larger value of  $a$  is expected from the running of the strong coupling constant. Attempts to parameterize the dependence of the rapidity loss as  $\sim -a/(\tau/\tau_0) + b(\tau/\tau_0) + c$  did not describe the data.

Therefore, the heavy quark mesons carry information on the distance dependence of the strong force. Plotting as in Fig. 3 the quark kinematic change ( $\Delta y$ ) as a function of the distance scale ( $\tau$ ) we see that information on the behaviour of the strong interaction potential between the quark–antiquark pair can be extracted directly from the data.

## 6 Fragmentation Distributions

In this section, the analysis is turned around and is used to predict fragmentation functions for hadrons which contain the primary quark and which have not decayed. The expected distributions of the energy change are obtained by folding the exponential proper time distribution (5) with the rapidity change as a function of the proper time determined in Fig. 3.

In Fig. 4, fragmentation functions are shown for different values of the scaling parameter  $\Delta y_0$ . The full curves give the situation where the quarks experience a rapidity loss according to

(10) together with  $C = 0.55$ . For the  $D^*$  data at  $\sqrt{s} = 10.6$  GeV, the dash-dotted curve shows the effect of the increased strength in the logarithmic term.

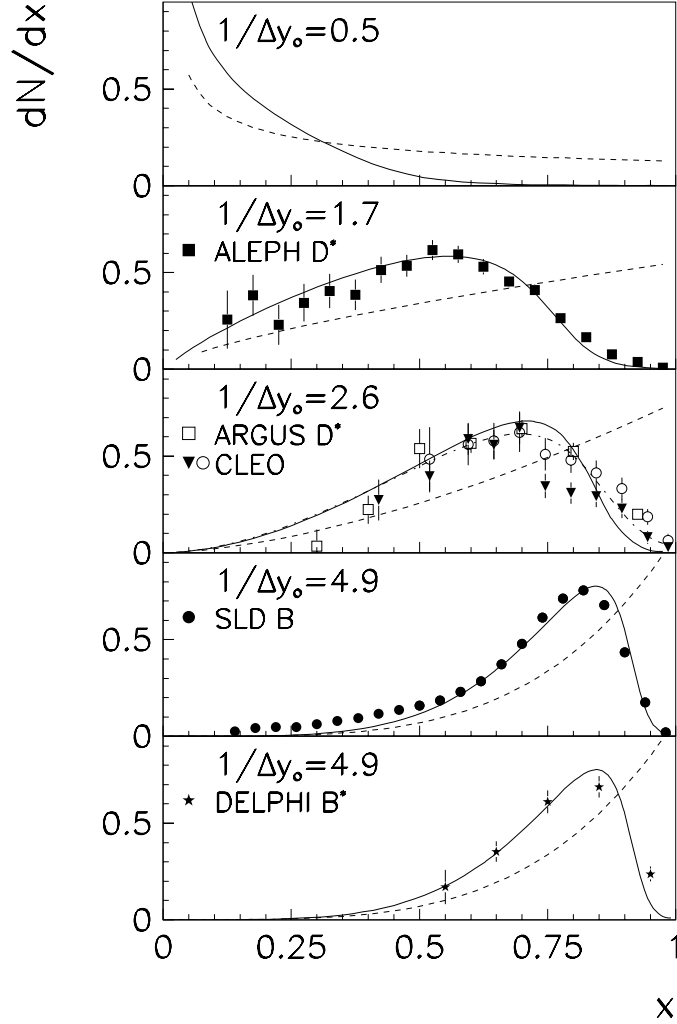


Figure 4: Fragmentation functions are shown for different values of the scaling parameter  $\Delta y_0$  and different situations: the dashed curves denote results from a linear dependence of the rapidity change on the time  $\tau$ . The full curves give the energy loss of a logarithmic plus linear dependence (10). In the middle plot, the dash-dotted curve shows the effect of an increased strength in the logarithmic term. The symbols represent the shapes of measured fragmentation distributions.

It is instructive to also consider the situation where a linear relation  $\Delta y \propto \tau$ , i.e. a constant force, is responsible for the fragmentation distributions (dashed curves). In this case, the rapidity distribution is exponentially falling (eqs. (3, 4, 5)), leading to energy distributions of the power law form

$$\frac{dN}{dx} \sim x^{[1/\Delta y_0 - 1]} \sim x^{[m/(\kappa\tau_0) - 1]} . \quad (11)$$



For accelerated masses  $m = \kappa\tau_0$ , the  $x$ -distributions are expected to be flat. For  $m > \kappa\tau_0$  and  $x \rightarrow 1$  the  $x$ -distributions are expected to increase and for  $m < \kappa\tau_0$  to decrease. As an example of the latter case, the upper figure shows the prediction for strange mesons, assuming  $1/\Delta y_0 = 0.5$  which corresponds to  $m = 0.25$  GeV at  $\kappa\tau_0 = 0.5$  GeV.

As a consequence of choosing  $x$  as the standard fragmentation observable for the hadrons considered here, light and heavy flavour fragmentation processes seem to be very different. Alternatively, using  $\Delta y$  as the fragmentation observable the spectra are expected to differ only by a scaling parameter.

## 7 Concluding Remarks

Measurements of heavy quark production in  $e^+e^-$  collisions have been analysed in terms of the quark rapidity change. The  $D^*$ ,  $B^*$ , and  $B$  meson spectra are found to follow a universal shape when expressed in units of a scaling parameter.

The shapes of the measurements are suggestive of a hadronization mechanism which is probabilistic in nature. Taking the view that the probability of hadron formation is constant in the rest frame of the travelling quark, the accelerated masses were determined. In principle, the measurements could be much improved by dedicated analyses using the original event data. A determination of the strange quark mass is desirable from measurements of kaons which are directly produced in  $e^+e^- \rightarrow s\bar{s}$  processes.

Furthermore, the mesons carry information on the variations in the strength of the quark–antiquark interactions. Directly from the data, information on the behaviour of the strong interaction potential between quark–antiquark pairs was extracted. It remains for ways to be found to compare the measurements to QCD lattice calculations. It will be of great interest to determine the potential between quarks and di-quarks from measurements involving protons. Comparisons of baryon spectra in central and peripheral collisions of heavy nuclei may be used in searches for the quark–gluon plasma where the field strengths are expected to be different.

Within the perspective of colour charged objects, losing energy in a known strong field for some time before they hadronize, fragmentation distributions of particles which contain the primary quark and which have not decayed can be viewed as essentially depending on the mass accelerated in the field.

## Acknowledgements

For very constructive, fruitful discussions and comments I wish to thank G. Barker, J. Dainton, M. Feindt, S. Kappler, P. Schleper, and T. Walter. I wish to thank Th. Müller and the IEKP group of the University Karlsruhe for their hospitality, and the Deutsche Forschungsgemeinschaft for the Heisenberg Fellowship.

## References

- [1] CLEO Collab., D. Bortoletto et al., *Phys. Rev.* **D37** (1988) 1719
- [2] ARGUS Collab., H. Albrecht et al., *Z. Phys.* **C52** (1991) 353
- [3] ALEPH Collab., R. Barate et al., *Eur. Phys. J.* **C16** (2000) 597
- [4] SLD Collab., Kenji Abe et al., *Phys. Rev. Lett.* **84** (2000) 4300
- [5] DELPHI Collab., P. Abreu et al., *Z. Phys.* **C68** (1995) 353
- [6] E. Eichten et al., *Phys. Rev. Lett.* **34** (1975) 369,  
*Phys. Rev.* **D17** (1978) 3090 and **D21** (1980) 203
- [7] W. Busza, T. Dreyer, M. Erdmann, *Z. Phys.* **C48** (1990) 167
- [8] T. Dreyer, M. Erdmann, *Phys. Lett.* **B260** (1991) 232
- [9] D.E. Groom et al., *Eur. Phys. J.* **C15** (2000) 1
- [10] DELPHI Collab., P. Abreu et al., *Phys. Lett.* **B418** (1998) 430
- [11] A. Brandenburg et al., *Phys. Lett.* **B468** (1999) 168
- [12] ALEPH Collab., R. Barate et al., *Eur. Phys. J.* **C18** (2000) 1